Hindawi
Adsorption Science & Technology
Volume 2022, Article ID 2885849, 10 pages
https://doi.org/10.1155/2022/2885849

Research Article

Hybrid PSf/TNT-SO_3H Ultrafiltration Membrane Fouling by Sodium Alginate: Effect of Permeation Flux on Fouling Resistance and Desalination Efficiency

Ibrahim Hotan Alsohaimi

Chemistry Department, College of Science, Jouf University, Sakaka 2014, Saudi Arabia

Correspondence should be addressed to Ibrahim Hotan Alsohaimi; ehalshaimi@ju.edu.sa

Received 9 May 2022; Accepted 29 August 2022; Published 9 September 2022

Academic Editor: Ming Hua

The development of low fouling UF membranes with boosting water flux for implementations in water purifications is critical. Organic foulants and ionic strength are the main characteristics of surface water which affect the membrane performance for water generation and seawater desalination. Low fouling hybrid ultrafiltration membranes were fabricated from a combination of sulfonic acid functionalized titanium nanotubes (TNTs-SO_3H) and polysulfone (PSf) by the nonsolvent-induced phase separation approach. The membrane fouling was explored utilizing a polysaccharide sodium alginate (SA) as a hydrophilic nature organic matter, and the impact of Na^+ and Ca^{2+} ions on alginate membrane fouling were also addressed. The results showed that the membranes' water permeability and natural organic matter fouling resistances were affected by the proportion of TNTs-SO_3H in the membranes. The inclusion of TNTs-SO_3H improves the water penetration fluxes (Jw1) and surface hydrophilicity of the manufactured membranes. In the UF of sodium alginate solution, the produced membrane comprising 5% TNTs-SO_3H exhibits a higher penetration flux and rejection value than the other membranes. The introduction of Na^+ and Ca^{2+} ions to the SA solution reduces the membrane fouling. Furthermore, the adsorption investigation of sodium alginate solutions at pH = 7 was lowered as the amount of TNTs-SO_3H was increased. After ultrafiltration, the fouled membrane containing 5% TNTs-SO_3H is readily removed, and recurrent antifouling experiments indicate a consistent and maximum filtration efficiency.

1. Introduction

The two primary sources of water-treatment technologies associated with the membrane process are drinking potable water and treatment of wastewater. Microbial products and natural organic matter were thoroughly shown to be important foulants generating membrane fouling in these implementations. Alginate is the most extensively utilized model foulant for membrane fouling studies due to its comparable fouling characteristics to microbial products and natural organic matter, as well as its abundance in natural settings. As a result, alginate was utilized to represent polysaccharides, which are plentiful in microbial products and natural organic matter. The research of alginate fouling behaviours is both easy and conducive to revealing general fouling processes.

Membrane fouling is connected directly to hydrophobicity, which can be successfully minimized by enhancing membrane hydrophilicity. Surface grafting and mixing approaches are being employed to improve the hydrophilicity of membranes [1, 2]. However, surface treatment, particularly grafting or adsorption of hydrophilic polymers, is not an accepted approach since changed membrane flow is reduced due to narrowing and blockage of surface pores. Because of its ease of use and the availability of a large variety of inorganic fillers, the blending approach has recently received a lot of attention for improving membrane hydrophilicity [3–6]. As inorganic fillers, ZrO_2, TiO_2, Al_2O_3, and CNTs were examined for use in the fabrication of low UF membranes with increased water flux and antifouling ability [7, 8]. The miscibility of polymer blends is of enormous

importance. The heat of blending is the primary factor of homogeneity. Exothermic mixing outweighs the positive equation-of-state impact on blending thermodynamics [9].

Titanium dioxide nanoparticles, especially, have piqued the interest of researchers for their potential use in the production of hybrid ultrafiltration membranes and photocatalysts in water purification [7, 10, 11]. Nonetheless, TiO_2 nanoparticle-derived hybrid ultrafiltration membranes have some intrinsic and important drawbacks, which are as follows: (i) TiO_2 nanoparticles in membrane casting solutions agglomerate at high concentrations; (ii) hydrophilicity and water flux are reduced at high fractions of TiO_2 nanoparticles due to defective pore structure formation in hybrid membranes; and (iii) TiO_2 nanoparticles from the membrane matrix can be leached. As a result, it is critical to develop an alternative to TiO_2 nanoparticles for use as an inorganic filler to improve the antifouling ability, water flux, and mechanical and thermal durability, of hybrid ultrafiltration membranes.

Because of their unique features, 1-D nanostructured TiO_2 with varied morphologies such as nanowires, nanofibers, nanorods, and nanotubes have piqued the interest of academic and industrial researchers. Nanostructured TiO_2 with a variety of morphologies has been investigated in various applications. TiO_2 nanotubes also exhibit hollow core/shell architectures, large specific surface areas, a high length-to-diameter ratio, and changeable surface characteristics [10, 12, 13]. As a result, TiO_2 nanotubes (TNTs) with a great ratio of length/diameter will overcome the aforementioned issues and will be useful in the preparation of low composite UF membranes with better water flow and antifouling fouling ability.

The development of low fouling UF membranes with rising water flux and selectivity for use in water purification is therefore of considerable interest. In this work, low fouling hybrid ultrafiltration membranes were fabricated from a combination of sulfonic acid functionalized titanium nanotubes (TNTs-SO_3H) and polysulfone (PSf) by nonsolvent-induced phase separation approach. The membrane fouling was explored utilizing sodium alginate (SA) as a hydrophilic nature organic matter rather than a hydrophobic humic acid. Furthermore, ions such as Na^+ and Ca^{2+} ions cannot be rejected effectively by membranes, but they may have a significant impact on fouling of the membrane through combinations with organic substances; therefore, the influence of Na^+ and Ca^{2+} ions on alginate membrane fouling was also addressed.

2. Experimental

2.1. Chemicals. Polysulfone (PSf) was obtained from Solvay (UDEL, P-3500 LCDMB7, Belgium). Polyvinylpyrrolidone (PVP), mercaptopropyltrimethoxysilane (MPTMS, 95 wt.%), alginic acid sodium salt, and hydrogen peroxide (35 wt.%) were obtained from Sigma–Aldrich. Toluene and N-methylpyrrolidone (NMP) were obtained from Applichem, Germany. Disodium hydrogen phosphate and sodium dihydrogen phosphate dehydrate were purchased from Merck Chemical Co. Titanium dioxide nanoparticle (P25) was purchased from Degussa, Germany. The remaining solvents were of commercial grade and were utilized exactly as obtained. Milli-Q system (Millipore) was used for water purification.

2.2. Materials Synthesis

2.2.1. Preparation and Functionalization of the Titanium Dioxide Nanotubes. In two steps, titanium dioxide nanotubes (TNTs) were synthesized and functionalized as described in the literature [14, 15]. First, TNTs were synthesized by hydrothermal approach in alkaline medium. Typically, titanium powder (P; 25 nm, 4 g) was blended with 100 mL solution of NaOH (10 M) overnight. The milky solution was then transferred into 200 mL PTFF lined autoclave, and the combination was hydrothermally treated for 24 h at 150°C. Following the hydrothermal process, the slurry was filtered and rinsed with (0.1 M) HCl and DI water till the pH of the rising solution reached around 6. The washed samples were dried for 8 h at 80°C and grounded to obtain fine TNT powder. In the second step, the functionalization of TNTs was carried out utilizing MPTMS precursor as the sulfonic acid moiety [16]. The reaction was performed under reflux conditions for 24 hours in toluene at 110°C, in molar ratios (1 : 2 : 200) of TNTs, MPTMS, and toluene, respectively, before being filtered and held in oven for 10 hours. The grafted mercapto moiety was then converted to –SO_3H moieties in H_2O_2 solution (35 wt.%) for 24 hours at 25°C. Filtration was performed on the prepared samples. Prior to characterisation, samples were dried overnight.

2.2.2. Membrane Fabrication. NIPSF approach was used to create PSf and TNT-SO_3H hybrid membranes [1, 17]. Membrane casting solutions were made by sonicating for 30 minutes in an ultrasonic bath with varied quantities of TNTs-SO_3H (1–10 wt.%) as displayed in Table 1, proportional to the total quantity of PSf polymer in NMP. Following that, PSf was integrated into the solutions while being stirred continuously at ambient temperature, resulting in homogenous solutions. The casting solutions were subsequently agitated at room temperature for 24 hours to enhance the dispersion of TNTs-SO_3H in the casting solutions. Using a casting knife, the solutions subsequently cast onto a clean glass plate with a thickness of 200 m. Following 30 seconds, the cleaned plate with the primitive coating was soaked in pure water until the membrane was removed which was then submerged in a pure water bath at ambient temperature to eliminate any NMP traces until the next characterisation and use. Membranes with varying TNT-SO_3H fractions (0, 1, 2, 5, and 10 wt.%) (Table 1) are labelled, respectively, as M-0, M-1, M-2, M-5, and M-10.

2.3. Membrane Characterisations. Membrane water absorption (φ) and porosity (ε) were evaluated using the reference [17]. The textural and cross-section morphologies of the prepared membrane were recorded utilizing a scanning electron microscope (Quanta 400 FEG, Czech Republic) at a voltage of 20 kV using various magnifications. The FTIR spectra of the fabricated membranes were acquired with an IR Tracer-100 Shimadzu spectrometer within a range of

Table 1: The composition of casting solutions for the preparation of hybrid ultrafiltration membranes.

Membrane	PSf (wt.%)	TNTs-SO_3H (wt.%)*	NMP (wt.%)
M-0	18	0	82
M-1	18	1	81.98
M-2	18	2	81.96
M-5	18	5	81.91
M-10	18	10	81.82

*The percentage of TNTs-SO_3H is based on the total fraction of the PSf polymer in the casting solution.

400–4000 cm^{-1}. The sessile drop technique was used to estimate contact angles on an FTA 200 contact angle analyzer (First Ten Angstroms, Inc., USA) equipped with video recording. Membrane water content and thermal durability in wet and dry environments were determined using differential scanning calorimetry (DSC, Q200 series (TA instrument, USA)) in a nitrogen atmosphere at temperatures ranging from -30 to +30°C and a flow rate of 50 mL min^{-1} and a heating rate of 10°C min^{-1} and thermal gravitational analysis (TGA, QS series) at temperatures ranging from 25 to 700°C in a nitrogen atmosphere, with a flow rate of 50 mL min^{-1} and a heating rate of 20°C min^{-1}.

2.4. UF Performance. In this study, a dead-end UF cell was utilized. For 30 minutes, each fabricated membrane was pressurized at 2 bars with pure water before being lowered to 1 bar. Following that, 1 hour of pure water was fed at 1 bar within the membranes, and the obtained permeate weight of this period was determined. Equation (1) was utilized to compute the water flux (Jw) of the membranes:

$$\mathrm{Jw} = \frac{m}{\rho \times A \times t}, \tag{1}$$

where m is the obtained permeate weight, A is the area of the membrane, t is the collection time, and ρ is the water density. By flowing 500 mL protein solution of sodium alginate (100 mg L^{-1}) at 1 bar and pH = 7, UF measurements were performed at ambient temperature with stirring speed of 400 rpm to test the antifouling performance. Following the protein solution UF, the used membranes have been completely rinsed in the cell by flowing pure water for 1 hour. The cell was subsequently supplied with DI water, and the water flux of the cleansed membranes was measured once more. The flux recovery ratio (FRR) of the membranes was calculated utilizing the following equation [17–19]:

$$\mathrm{FRR}\,(\%) = \frac{\mathrm{Jw2}}{\mathrm{Jw1}} \times 100, \tag{2}$$

where Jw1 is the membrane's initial water flux and Jw2 is the cleaned membrane's water flux after UF of sodium alginate protein solution. The following equations are often utilized to determine the antifouling performance of the fabricated membranes in order to thoroughly examine the fouling mechanism. Equations (3), (4), and (5) were used to compute the total fouling ratio (Rt), reversible fouling ratio (Rr), and irreversible fouling ratio (Rir):

$$\mathrm{Rt} = \frac{\mathrm{Jw1} - \mathrm{Js}}{\mathrm{Jw1}} \times 100, \tag{3}$$

$$\mathrm{Rr} = \frac{\mathrm{Jw2} - \mathrm{Jx}}{\mathrm{Jw1}} \times 100, \tag{4}$$

$$\mathrm{Rir} = \frac{\mathrm{Jw1} - \mathrm{Jw2}}{\mathrm{Jw1}} \times 100, \tag{5}$$

where Js is the membrane's sodium alginate flux.

2.5. Adsorption Investigation. The adsorption studies were carried out to quantify the quantity of sodium alginate adsorbed on the membranes at a neutral medium (pH = 7). The adsorption capacity per unit area of the membrane (q) was calculated using Equation (6). Sodium alginate concentrations were determined using a UV-Vis spectrophotometer (a Cary 50 Probe, Varian Inc.) at 200 nm.

$$q = \frac{(C_o - C_t)V}{A}, \tag{6}$$

where C_o and C_t are the original and final sodium alginate concentrations, respectively, A and V are the real membrane area and the sodium alginate volume applied in the adsorption measurements, respectively.

3. Results and Discussion

3.1. Membrane Characterisation

3.1.1. Morphology of the Membrane. The fabrication approach and materials utilized have the greatest influence on the architecture of the membrane. The membrane architecture provides valuable information on the porosity, flux, and membrane pore size distribution. Cross-section SEM images of the fabricated membrane containing various quantities of TNTs-SO_3H were collected in this investigation (Figures 1(a)–1(e)). The morphology seems to be devoid of macroscopic defects, since it resembles that of typically UF membranes. Furthermore, the M-0 surface's SEM image exhibits a uniform and consistent surface with an uneven pore pattern with sponge-like porosity (Figure 1(a)). Although, the fabricated membrane cross-section exhibits a different morphology from the M-0 image. The fabricated membranes have a porous architecture with a high extent of interconnectivity (Figures 1(b)–1(d)). The membrane porosity was promoted with an increasing quantity of TNTs-SO_3H in the casting solutions, as displayed in the membrane's cross-sectional images. This effect was obviously noticed during the synthesis of the prepared membranes from the casting solutions having varying amounts of TNTs-SO_3H. Among all membranes, M-10 appeared to have the highest porosity of any membrane tested. These results indicate that the introduction of TNTs-SO_3H had a considerable effect on the membrane development owing to various parameters like surface functional moieties,

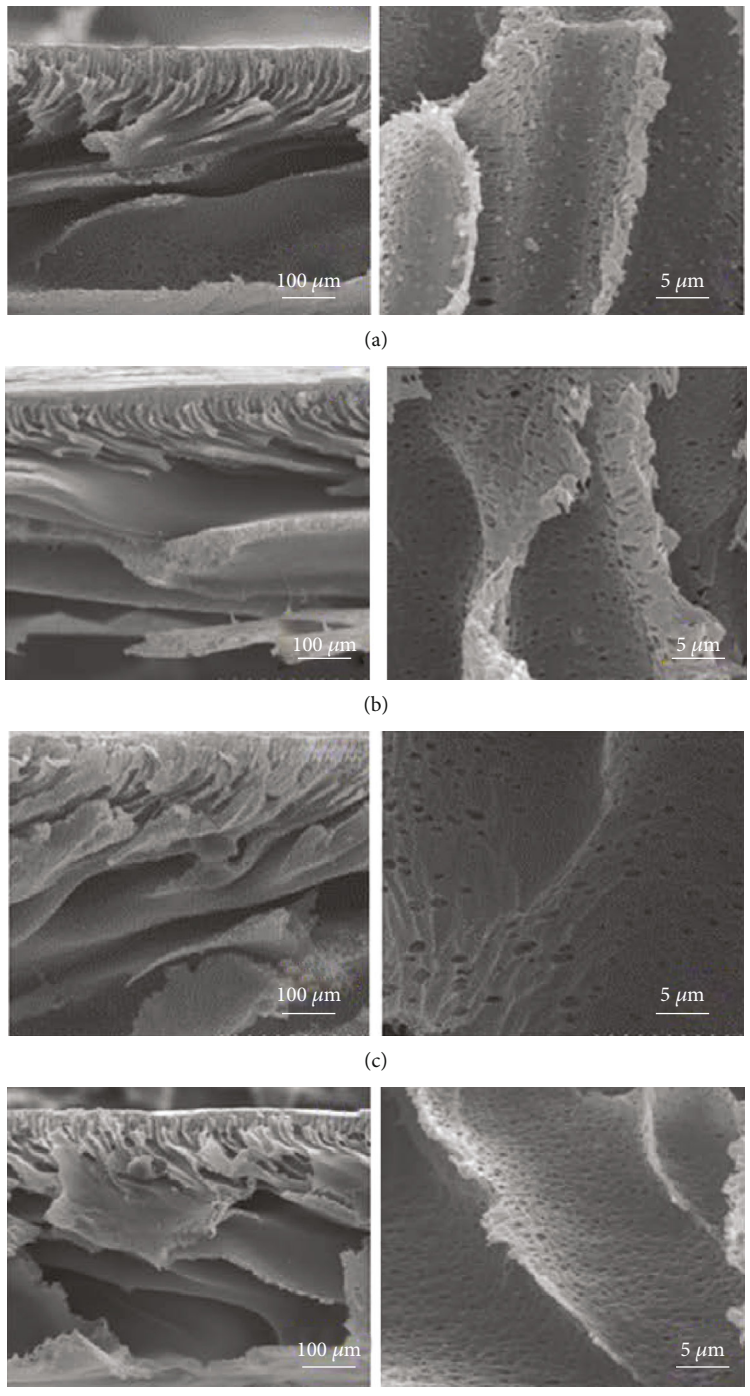

Figure 1: Continued.

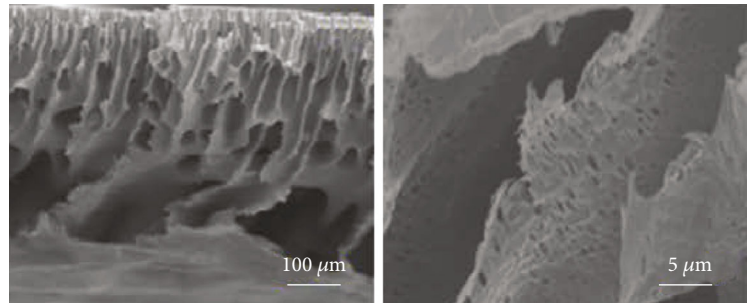

(e)

Figure 1: The cross-section SEM images of PSf/TNTs-SO_3H membranes prepared with various amounts of TNTs-SO_3H (a) M-0, (b) M-1, (c) M-2, (d) M-4, and (e) M-10.

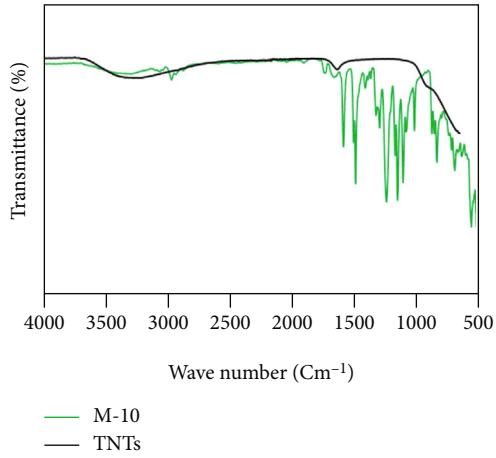

Figure 2: FTIR spectra for pure TNTs and M-10 membrane.

Table 2: Physicochemical characteristics comprising porosity water uptake, contact angles, and the surface ζ at pH = 7 for the fabricated ultrafiltration membranes.

Membrane	φ (%)	ε (%)	Contact angle θ (°)	ζ (mv)
M-0	66.25	38.74	77.83	-11.2
M-1	72.38	38.97	73.72	-14.6
M-2	75.5	48.42	71.39	-16.2
M-5	77.14	56.60	70.27	-18.7
M-10	78.18	64.37	60.1	-21.7

surface charge, and concentration of active centres. This is could be due to the solvent (NMP) exchange rate with the nonsolvent (water) during the inversion process. The rate of exchange of water with NMP was increased when the casting solution's hydrophilicity rose.

3.1.2. Spectroscopic Properties. Figure 2 depicts the membrane's ATR-FTIR spectra of pure TNTs and M-10 membrane. The wide characteristics bands in the range of 3280-3400 cm^{-1} are ascribed to the stretching mode of hydroxyl moieties on tubular TiO_2. Besides, the Ti-O-Ti existing in TNTs are responsible for the absorption peak at 1650 cm^{-1}. The bands at 2878 and 3017 cm^{-1} are ascribed to the aliphatic and aromatic modes of $-CH_2$ moieties. The absorption peaks at 1570 and 1480 cm^{-1} are assigned to the stretching modes of aromatic molecules. The characteristics peak at 1143 cm^{-1} related to the linkage of ether. The stretching modes of $-SO_3$ moieties in the membrane are responsible for the distinctive bands at 1315, 1246, and 1050 cm^{-1}.

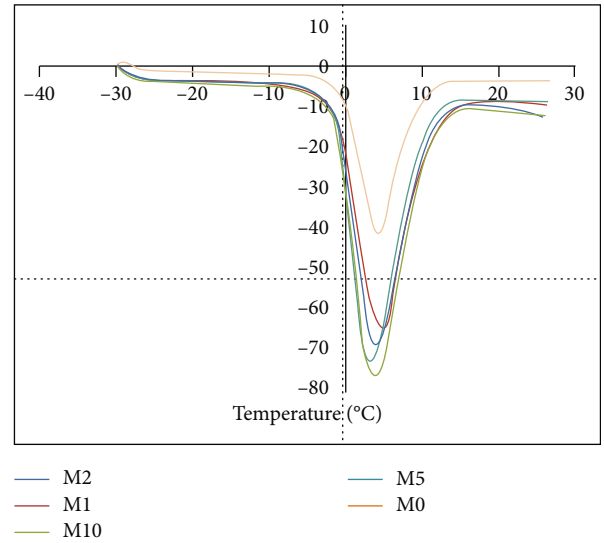

Figure 3: DSC heating curves for membranes with different water contents at temperature range -30–+30°C.

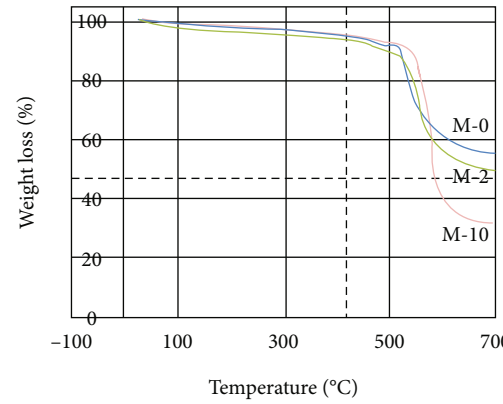

Figure 4: TGA curves of membranes: M-0, T_d 499.45°C; M-2, T_d 530.50°C; M-10, T_d 518.66°C.

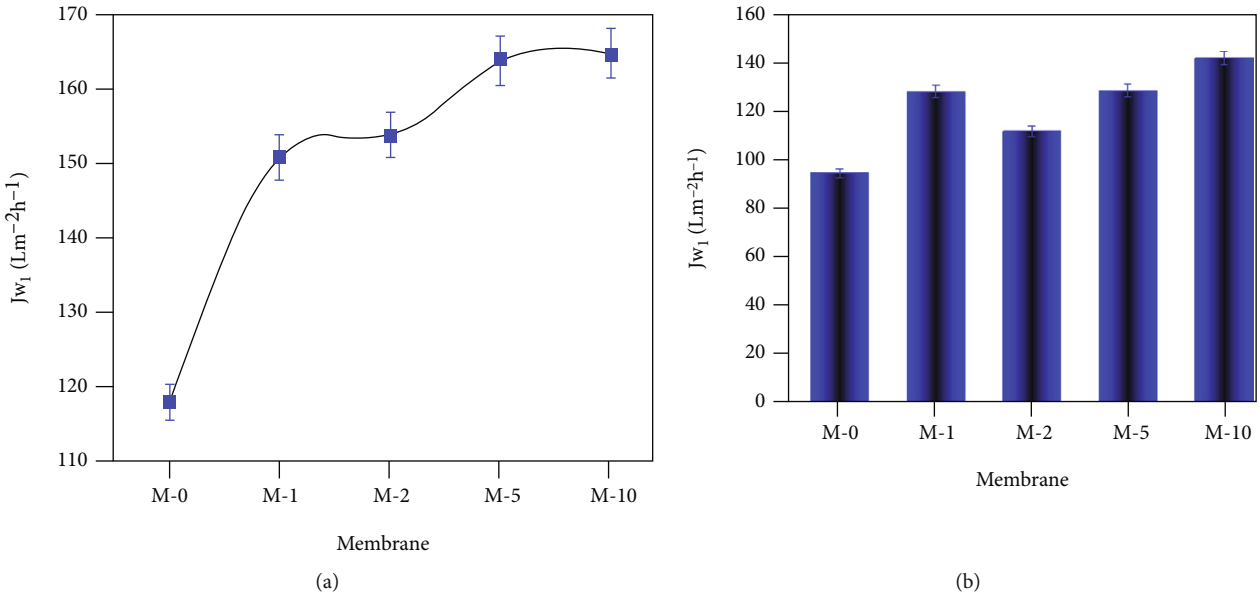

FIGURE 5: (a) Pure water flux and (b) sodium alginate solution fluxes for the hybrid UF membranes at pH = 7, applied pressure (1 bar), and a stirring speed (400 rpm).

These findings support the incorporation of TNTs-SO_3H into the hybrid membrane framework [20–24].

3.1.3. Membrane Hydrophilicity. The membrane hydrophilicity was assessed by evaluating their water contact angles with the sessile drop approach, which is recommended for porous membranes since it allows for analysis while being completely hydrated [25, 26]. Table 2 displays the obtained values. The results show that the water contact angle values were affected by the percentage of TNTs-SO_3H in the membranes. The maximum contact angle (77.38°) was found for the pristine membrane (M-0), which could be attributable to the lack of –SO_3H hydrophilic moieties on the membrane. As the TNT-SO_3H percentage in the membranes grew, the contact angle values decreased progressively. This is due to the development of a compact layer of hydration on the surface of the membrane as a result of the –SO_3H groups' increased affinity for water and TNT-enhanced water uptake capacity. The membrane surfaces have become more hydrophilic after the addition of TNTs-SO_3H. Membrane M-10 had the lowest angle of contact (60.1°), which corresponded to the highest hydrophilicity as determined by the values of water uptake (Table 2). These findings suggest that by altering the proportion of TNTs-SO_3H in polymer mix casting solutions, the membrane hydrophilicity can be regulated.

3.1.4. Thermal Investigation. Further assessments were performed to verify the thermal water content properties. The DSC investigations were all carried out at temperatures ranging from -30 to +30°C. Figure 3 depicts the DSC profiles for the composite membranes. All the fabricated membranes displayed the endothermic event due to the moisture absorption. The water evaporation at high temperatures from the membrane is linked to the DSC heating curves. Furthermore, the peak area of the membranes rose correspondingly with the quantity of TNTs-SO_3H. These findings support the produced membranes' hydrophilicity promote through water uptake, contact angle, and porosity.

The thermal stability of the fabricated membranes M-0, M-2, and M-10 is displayed in Figure 4. It is worth noting that all fabricated membranes displayed the initial weight loss at 105°C due to the removal of the adsorbed moisture. In addition, the mass loss was between 490 and 535°C for all membranes, and the greater thermal breakdown temperature T_d for the modified membranes compared to the membrane M-0 suggested a stronger thermal stability of the composite membranes. This might be attributed to the fixing of the chain of polymer owing to the presence of the nanofiller which hinders the polymer chain mobility and degradation at higher temperatures.

3.1.5. Membrane Surface Charge. Streaming potential measurements were used to assess the influence of TNTs-SO_3H loading on the surface charge of fabricated membranes at various TNT-SO_3H concentrations. Table 2 displays the acquired surface charge ζ (mV) values at pH = 7. It can be seen that the surface charge ζ (mV) of pristine membrane M-0 was negative (-11.2 mV) at pH = 7. The surface ζ (mV) values were increased further as the quantity of TNTs-SO_3H increased. The presence of extra –SO_3H groups in the barrier layer of hybrid membrane M-10 resulted in the highest surface charge (-21.7 mV).

3.2. Membrane Efficiency

3.2.1. Permeability. To assess the effect of the nanoparticle on water permeability, the pure water flux (Jw) was monitored as shown in Figure 5(a). The Jw magnitude for the modified membranes was significantly boosted as the quantity of TNTs-SO_3H in the membranes rose. The magnitude

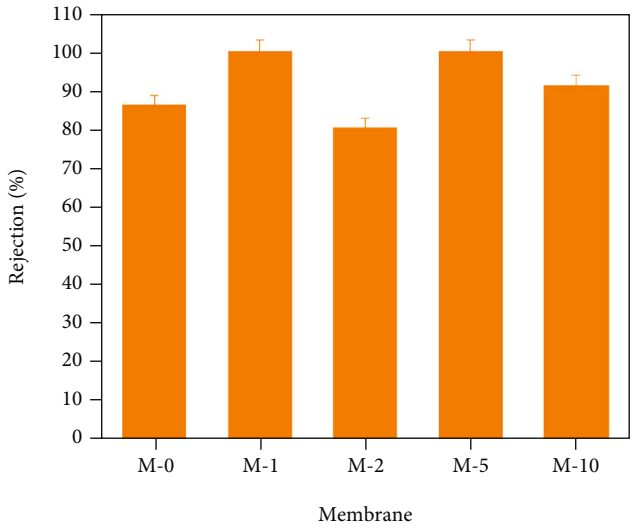

Figure 6: Rejection of sodium alginate on the ultrafiltration membranes at pH = 7.

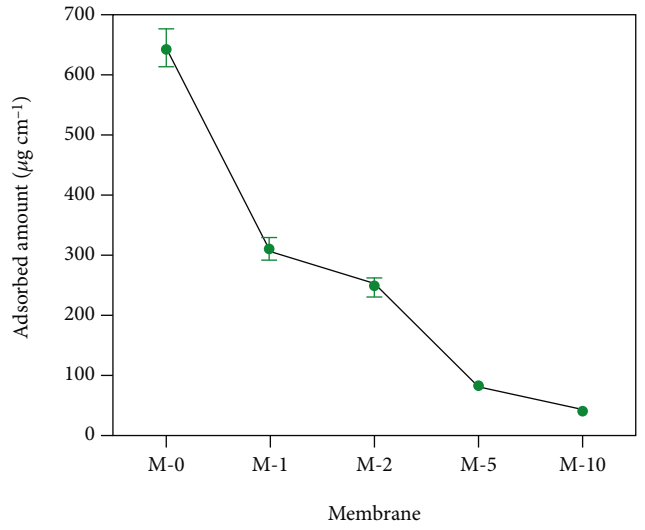

Figure 7: Adsorption of sodium alginate solution (100 mg L^{-1}) at pH = 7 on the UF membranes.

of Jw for membrane M-0 was reported to be 118 L m^{-2} h^{-1} that is less than the magnitude for fabricated membranes. This is connected to the smallest membrane density, M-0. Membrane M-10 had the greatest value of Jw for the hybrid membranes (165 L m^{-2} h^{-1}) because it had the maximum hydrophilicity, water absorption, and porosity (Table 2). Moreover, the Jw magnitude for the M-1 membrane was reported to be 151 L m^{-2} h^{-1} that is smaller than the flux for composite membranes. This could be due to the smallest TNT-SO_3H percentage which resulted in poorer porosity and water uptake. The proportion of TNTs-SO_3H in the membrane similarly affected sodium alginate solution fluxes (Jx) (Figure 5(b)). The Jx magnitude was boosted significantly with increasing quantity of TNTs-SO_3H, as expected, and the greatest Jx (Sod. Alg.; 142 L m^{-2} h^{-1}) magnitude was recorded for the M-10 membrane. However, for all membranes, Jx values were lower than Jw values; this could be attributed to the polarization gradient and the solution fouling, which are explored in detail below. It was also reported that in the membrane as the quantity of TNTs-SO_3H rose, the solution rejection increased somewhat. The membrane M-5 has the greatest rejection scores (Figure 6). However, a large TNT-SO_3H fraction (10 wt.%) generated a modest decrease in membrane performance, which may also be very closely connected with the impacts of NIPSF conditions on the pore structure of the membrane.

3.2.2. Ultrafiltration Performance. The membranes' ultrafiltration efficiency was assessed using sodium alginate solution flux recovery ratio and adsorption. The ultrafiltration performance of hybrid membranes was investigated using sodium alginate solutions in this work. Figure 7 depicts the adsorbed quantities of sodium alginate at neutral medium (pH = 7). The adsorbed amounts of sodium alginate were lowered for membranes containing a high quantity of TNTs-SO_3H; the observed behaviour is in agreement with the angles of contact (Table 2). Because the compact layer

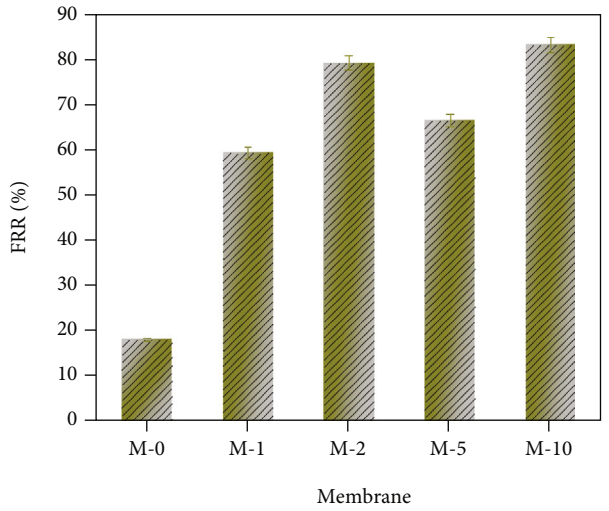

Figure 8: Flux recovery ratio for the ultrafiltration membranes after UF of sodium alginate solution (100 mg L^{-1}) and subsequent washing with DI water.

Table 3: The summary of total fouling ratio (Rt), the reversible fouling ratio (Rr), and the irreversible fouling ratio (Rir) for the blend membranes.

Membrane	Rr (%)	Rir (%)	Rt (%)
M-0	4.13	56.31	58.22
M-1	5.09	23.16	28.25
M-2	6.18	20.79	26.98
M-5	8.18	12.71	20.90
M-10	11.19	2.58	13.77

of hydration on the surface of the membrane blocked the interaction of the adsorbed quantities of sodium alginate with the surface, the effective decrease in the adsorbed quantity of sodium alginate happened [19]. Under similar experimental circumstances, the membrane M-10 was less prone

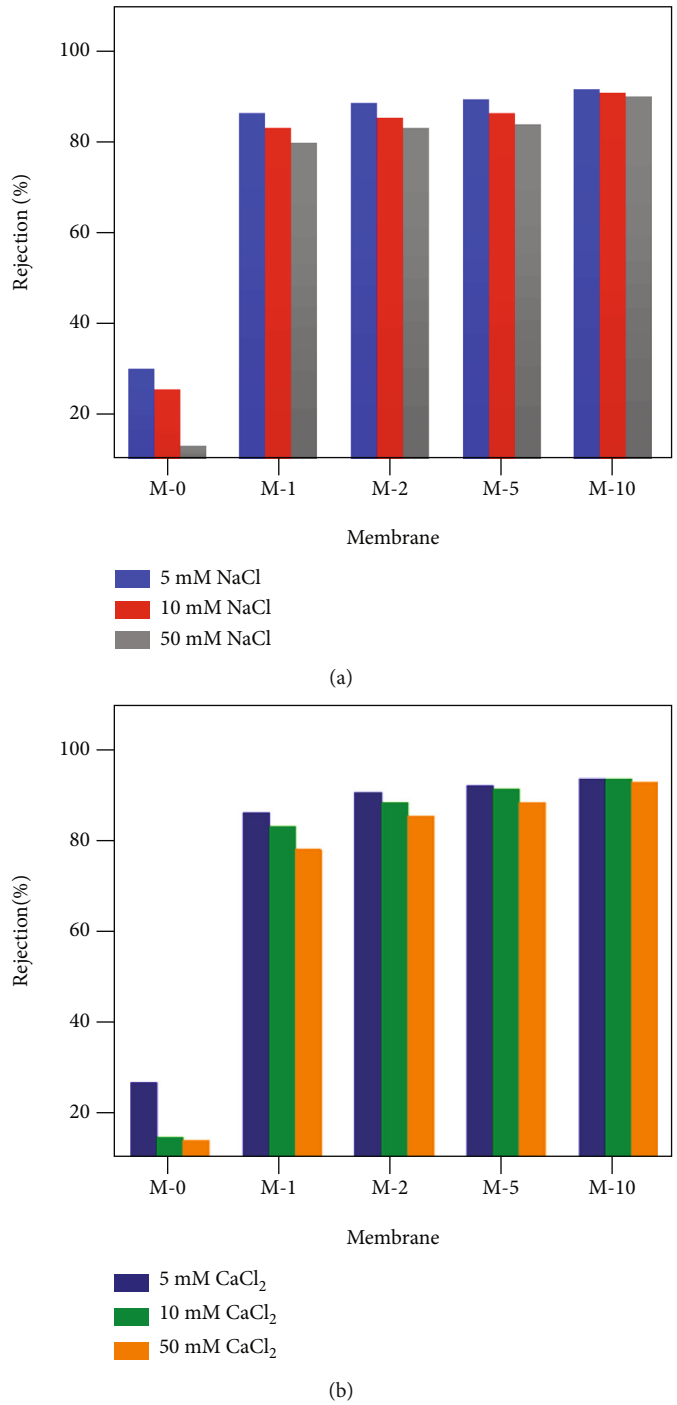

Figure 9: Rejection (%) when filtering SA in the presence of different concentrations of (a) NaCl and (b) $CaCl_2$.

to sodium alginate adsorption than any other membranes. The smallest value recorded for the adsorbed amount of sodium alginate solutions on the membrane M-10 at neural medium (pH = 7) was 41.6 g cm^{-2} (Figure 7). Due to their great binding ability of water, the greatest quantity of TNTs-SO_3H may have formed the most appropriate layer of hydration on the whole surface [26]. The amount of sodium alginate solutions adsorbed on all hybrid membranes was less than on membrane M-0 (without TNTs-SO_3H). As a result, low fouling would be appropriate for protein solutions UF at pH = 7. Figure 8 shows membranes' FRR after UF of sodium alginate solutions at neutral medium (pH = 7). The FRR magnitude for pristine membrane after sodium alginate UF at neutral medium is determined to amount to 39%, the smallest of all membranes. This due to the generated fouling by hydrophobic combination of sodium alginate solutions and PSf in the membrane [17, 19, 20]. The FRR values were enhanced further as the quantity of TNTs-SO_3H was boosted. Summing up, FRR values for the composite membranes were higher than those

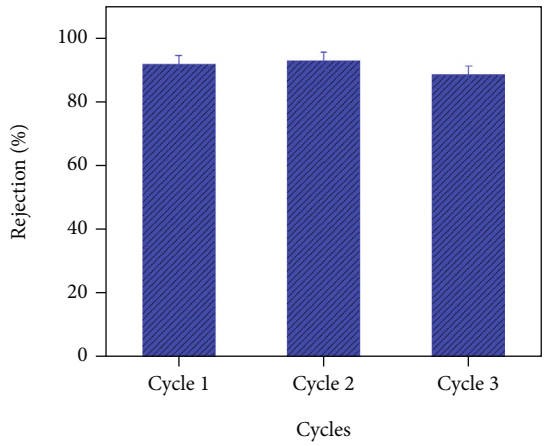

Figure 10: Sodium alginate rejection in fouling cycles on membrane M-5.

for pristine membrane M-0 (without TNTs-SO_3H), indicating that the membrane's antifouling ability of the PSf was boosted following the introduction of TNTs-SO_3H. The hybrid membrane's high FRR values imply that the uptake protein on the surface of the membrane can be easily detached by cleaning with water. The fouling behaviour of the fabricated membranes was explored further by computing the Rt, Rr, and Rir, as shown in Table 3. The findings show that as the quantity of TNTs-SO_3H increased, Rt values for sodium alginate solution decreased significantly. The Rr magnitude rose with a quantity of TNTs-SO_3H, resulting in a decrease in the irreversible solution fouling ratio (Rir). Membrane M-5 was chosen to repeat the water flux and antifouling performance after washing with 0.1 M of NaOH solution under same conditions since this membrane obtained the highest rejection values.

It worth noting that with rising quantity of TNTs-SO_3H, the SA uptake efficacy of fabricated membranes was boosted. The difference in porosity of fabricated membranes at different TNT-SO_3H contents may be responsible for enhanced SA uptake performance. Because of the rise in $-SO_3H$ moieties in the membrane, the charged characteristics of the fabricated membranes increased with the rising content of TNTs-SO_3H. As a consequence, the similarly charged fabricated membrane successfully retained negatively charged foulant molecules at pH = 7, increasing its removal efficiency.

3.2.3. Influence of Na^+ and Ca^{2+} on UF Performance of SA. The presence of Na^+ monovalent ion and Ca^{2+} divalent ion had an influence on UF of SA solution under high salinity. Three different NaCl and $CaCl_2$ concentrations were examined (5, 10, and 50 ppm) (Figure 9). The rejection (%) increased in the presence of both NaCl and $CaCl_2$ with rising content of TNTs-SO_3H. Both Na^+ and Ca^{2+} ions have a significant impact on the UF of SA solution leading to fouling mitigation.

3.2.4. Reusability. The membrane M-5 was chosen for durability determination that comprises SA fouling and rinsing with DI water. Sodium alginate rejection in fouling cycles on membrane M-5 is presented in Figure 10. In the first cycle, the rejection (%) of the M-5 membrane was 92.08%. More obviously, the rejection (%) of the M-5 membrane was still maintained at 93.1 and 88.7% following the second and third fouling and washing runs, respectively. The rejection values were noticeably similar as compared to original values, which confirmed a steady and best filtration performance with addition of TNTs-SO_3H in the membranes. Besides, there is a strong interaction of TNTs-SO_3H in the fabricated membranes, and the nanofiller did not leach out during the UF tests.

4. Conclusion

The NIPSF approach was explicit to successfully modify reduced fouling fabrication of ultrafiltration membranes comprised of TNTs-SO_3H and polysulfone (PSf) blends. The membranes have a standard asymmetric shape with a porous sublayer and a thin layer. The findings of ultrafiltration tests show that the addition of TNTs-SO_3H had a significant impact on membrane ultrafiltration performance due to features such as surface functional moieties, active centres, and surface charge. In the casting solutions, by adjusting the proportion of TNTs-SO_3H at an extremely small magnitude relative to the polymer matrix, the membrane porosity and hydrophilicity could be regulated. The membranes have become less susceptible to sodium alginate adsorption. The fouling characteristics of the membranes was dramatically decreased as the quantity of TNTs-SO_3H was increased. Thus, by altering the proportion of TNTs-SO_3H, the hybrid membranes' sodium alginate solution adsorption and fouling characteristics could be controlled. Sodium alginate fluxes were substantially based on the quantity of TNTs-SO_3H in the membranes, with membrane M-10 yielding the highest values. At pH = 7, membrane M-5 had the highest rejection values of sodium alginate solution through the membranes. When the rejection and FRR values of pristine and composite membranes are compared, it is clear that the performance of the antifouling is enhanced with the introduction of TNTs-SO_3H. Furthermore, the discovered membranes could be used to remove protein and natural organic materials from wastewater.

Data Availability

The data used to support the findings of this study are available from the corresponding author upon request.

Conflicts of Interest

The author declares that they have no conflicts of interest.

Acknowledgments

The author appreciatively acknowledges the Chemistry Department, Jouf University, for access to the analytical equipment.

References

[1] Y. Liao, T. P. Farrell, G. R. Guillen et al., "Highly dispersible polypyrrole nanospheres for advanced nanocomposite ultrafiltration membranes," *Materials Horizons*, vol. 1, no. 1, pp. 58–64, 2014.

[2] D. G. Kim, H. Kang, S. Han, H. J. Kim, and J. C. Lee, "Bio- and oil-fouling resistance of ultrafiltration membranes controlled by star-shaped block and random copolymer coatings," *RSC Advances*, vol. 3, no. 39, pp. 18071–18081, 2013.

[3] M. Kumar and M. Ulbricht, "Advanced ultrafiltration membranes based on functionalized poly(arylene ether sulfone) block copolymers," *RSC Advances*, vol. 3, no. 30, pp. 12190–12203, 2013.

[4] D. Rana, T. Matsuura, R. M. Narbaitz, and C. Feng, "Development and characterization of novel hydrophilic surface modifying macromolecule for polymeric membranes," *Journal of Membrane Science*, vol. 249, no. 1-2, pp. 103–112, 2005.

[5] D. Rana, T. Matsuura, and R. M. Narbaitz, "Novel hydrophilic surface modifying macromolecules for polymeric membranes: polyurethane ends capped by hydroxy group," *Journal of Membrane Science*, vol. 282, no. 1-2, pp. 205–216, 2006.

[6] Y. Kim, D. Rana, T. Matsuura, and W. J. Chung, "Towards antibiofouling ultrafiltration membranes by blending silver containing surface modifying macromolecules," *Chemical Communications*, vol. 48, no. 5, pp. 693–695, 2012.

[7] J. M. Arsuaga, A. Sotto, G. del Rosario et al., "Influence of the type, size, and distribution of metal oxide particles on the properties of nanocomposite ultrafiltration membranes," *Journal of Membrane Science*, vol. 428, pp. 131–141, 2013.

[8] M. Kumar and M. Ulbricht, "Novel antifouling positively charged hybrid ultrafiltration membranes for protein separation based on blends of carboxylated carbon nanotubes and aminated poly(arylene ether sulfone)," *Journal of Membrane Science*, vol. 448, pp. 62–73, 2013.

[9] D. Rana, K. Bag, S. N. Bhattacharyya, and B. M. Mandal, "Miscibility of poly (styrene-co-butyl acrylate) with poly (ethyl methacrylate): existence of both UCST and LCST," *Journal of Polymer Science Part B: Polymer Physics*, vol. 38, no. 3, pp. 369–375, 2000.

[10] R. Kumar, A. M. Isloor, A. F. Ismail, S. A. Rashid, and A. A. Ahmed, "Permeation, antifouling and desalination performance of TiO_2 nanotube incorporated PSf/CS blend membranes," *Desalination*, vol. 316, pp. 76–84, 2013.

[11] R. Molinari, L. Palmisano, E. Drioli, and M. Schiavello, "Studies on various reactor configurations for coupling photocatalysis and membrane processes in water purification," *Journal of Membrane Science*, vol. 206, no. 1-2, pp. 399–415, 2002.

[12] J. H. Jung, H. Kobayashi, K. J. C. van Bommel, S. Shinkai, and T. Shimizu, "Creation of novel helical ribbon and double-layered nanotube TiO_2 structures using an organogel template," *Chemistry of Materials*, vol. 14, no. 4, pp. 1445–1447, 2002.

[13] G. Niu, W. Liu, T. Wang, and J. Ni, "Absorption of Cr(VI) onto amino-modified titanate nanotubes using 2-bromoethylamine hydrobromide through S_N2 reaction," *Journal of Colloid and Interface Science*, vol. 401, pp. 133–140, 2013.

[14] H. Ou and S. Lo, "Review of titania nanotubes synthesized via the hydrothermal treatment: fabrication, modification, and application," *Separation and Purification Technology*, vol. 58, no. 1, pp. 179–191, 2007.

[15] T. Kasuga, M. Hiramatsu, A. Hoson, T. Sekino, and K. Niihara, "Formation of titanium oxide nanotube," *Langmuir*, vol. 14, no. 12, pp. 3160–3163, 1998.

[16] L. Wang, M. Yang, Z. Shi, Y. Chen, and J. Feng, "Two-dimensional metal-organic framework constructed from 4,4′-bipydine and 1,2,4-benzenetricarboxylate: synthesis, structure and magnetic properties," *Journal of Solid State Chemistry*, vol. 178, no. 11, pp. 3359–3365, 2005.

[17] M. Kumar and M. Ulbricht, "Novel ultrafiltration membranes with adjustable charge density based on sulfonated poly(arylene ether sulfone) block copolymers and their tunable protein separation performance," *Polymer*, vol. 55, no. 1, pp. 354–365, 2014.

[18] E. Celik, L. Liu, and H. Choi, "Protein fouling behavior of carbon nanotube/polyethersulfone composite membranes during water filtration," *Water Research*, vol. 45, no. 16, pp. 5287–5294, 2011.

[19] G. N. B. Barona, B. J. Cha, and B. Jung, "Negatively charged poly(vinylidene fluoride) microfiltration membranes by sulfonation," *Journal of Membrane Science*, vol. 290, no. 1-2, pp. 46–54, 2007.

[20] Y. Liu, X. Yue, S. Zhang et al., "Synthesis of sulfonated polyphenylsulfone as candidates for antifouling ultrafiltration membrane," *Separation and Purification Technology*, vol. 98, pp. 298–307, 2012.

[21] G. Yilmaz, H. Toiserkani, D. O. Demirkol et al., "Polysulfone based amphiphilic graft copolymers by click chemistry as bioinert membranes," *Materials Science and Engineering: C*, vol. 31, pp. 1091–1097, 2011.

[22] X. Y. Shang, D. Shu, S. J. Wang, M. Xiao, and Y. Z. Meng, "Fluorene-containing sulfonated poly(arylene ether 1,3,4-oxadiazole) as proton- exchange membrane for PEM fuel cell application," *Journal of Membrane Science*, vol. 291, no. 1-2, pp. 140–147, 2007.

[23] M. Wang, L. G. Wu, J. X. Mo, and C. J. Gao, "The preparation and characterization of novel charged polyacrylonitrile/PES-C blend membranes used for ultrafiltration," *Journal of Membrane Science*, vol. 274, pp. 200–208, 2006.

[24] G. Socrates, *Infrared Characteristic Group Frequencies*, Wiley, 1980.

[25] P. D. Peeva, T. Knoche, T. Pieper, and M. Ulbricht, "Cross-flow ultrafiltration of protein solutions through unmodified and surface functionalized polyethersulfone membranes – effect of process conditions on separation performance," *Separation and Purification Technology*, vol. 92, pp. 83–92, 2012.

[26] Y. Liao, X. G. Li, E. M. V. Hoek, and R. B. Kaner, "Carbon nanotube/polyaniline nanofiber ultrafiltration membranes," *Journal of Materials Chemistry A*, vol. 1, no. 48, pp. 15390–15396, 2013.